Nucl Med Mol Imaging (2014) 48:26–32
DOI 10.1007/s13139-013-0240-6

ORIGINAL ARTICLE

Evaluation of Dixon Sequence on Hybrid PET/MR Compared with Contrast-Enhanced PET/CT for PET-Positive Lesions

Ju Hye Jeong · Ihn Ho Cho · Eun Jung Kong · Kyung Ah Chun

Received: 13 May 2013 / Revised: 14 August 2013 / Accepted: 12 September 2013 / Published online: 15 October 2013

Abstract
Purpose Hybrid positron emission tomography and magnetic resonance (PET/MR) imaging performs a two-point Dixon MR sequence for attenuation correction. However, MR data in hybrid PET/MR should provide anatomic and morphologic information as well as an attenuation map. We evaluated the Dixon sequence of hybrid PET/MR for anatomic correlation of PET-positive lesions compared with contrast-enhanced PET/computed tomography (CT) in patients with oncologic diseases.
Methods Twelve patients underwent a single injection, dual imaging protocol. PET/CT was performed with an intravenous contrast agent (85±13 min after ^{18}F-FDG injection of 403±45 MBq) and then (125±19 min after injection) PET/MR was performed. Attenuation correction and anatomic allocation of PET were performed using contrast-enhanced CT for PET/CT and Dixon MR sequence for hybrid PET/MR. The Dixon MR sequence and contrast-enhanced CT were compared for anatomic correlation of PET-positive lesions (scoring scale ranging from 0 to 3 for visual ratings). Additionally, standardized uptake values (SUVs) for the detected lesions were assessed for quantitative comparison.
Results Both hybrid PET/MR and contrast-enhanced PET/CT identified 55 lesions with increased FDG uptake in ten patients. In total, 28 lymph nodes, 11 bone lesions, 3 dermal nodules, 3 pleural thickening lesions, 2 thyroid nodules, 1 pancreas, 1 liver, 1 ovary, 1 uterus, 1 breast, 1 soft tissue and 2 lung lesions were present. The best performance was observed for anatomic correlation of PET findings by the contrast-enhanced CT scans (contrast-enhanced CT, 2.64±0.70; in-phase, 1.29±1.01; opposed-phase, 1.29±1.15; water-weighted, 1.71±1.07; fat weighted, 0.56±1.03). A significant difference was observed between the scores obtained from the contrast-enhanced CT and all four coregistered Dixon MR images. Quantitative evaluation revealed a high correlation between the SUVs measured with hybrid PET/MR (SUVmean, 2.63±1.62; SUVmax, 4.30±2.88) and contrast-enhanced PET/CT (SUVmean, 3.88±2.30; SUVmax, 6.53±4.04) in PET-positive lesions (SUVmean, ρ=0.93; SUVmax, ρ=0.95), although hybrid PET/MR presented a decrease of SUVs compared with contrast-enhanced PET/CT (mean reduction; SUVmean, 32.44±15.64 %; SUVmax, 35.16±12.59 %).
Conclusions Despite different attenuation correction approaches, the SUV of PET-positive lesions correlated well between hybrid PET/MR and contrast-enhanced PET/CT. However Dixon MR images acquired for attenuation correction were insufficient to provide anatomic information of PET images because of low spatial resolution. Thus, additional MR sequence with fast and higher resolution may be necessary for anatomic information.

Keywords Positron emission tomography · Positron emission tomography and computed tomography · Magnetic resonance imaging · Fluorodeoxyglucose F-18 · Neoplasms

Introduction

A conventional positron emission tomography/computed tomography (PET/CT) scanner generates an attenuation map based on CT data and CT image helps diagnostic interpretation of PET/CT

J. H. Jeong · I. H. Cho (✉) · E. J. Kong · K. A. Chun
Department of Nuclear medicine, Yeungnam University Hospital, #317-1 Daemyung 5-dongNam-gu Daegu 705-717, Republic of Korea
e-mail: ihcho@med.yu.ac.kr

as an anatomical framework. Accurate anatomic localization of functional abnormalities on PET scan is challenging because of limited anatomical information and low spatial resolution. However, the integration of functional and anatomical information in PET/CT has resulted in significant improvement in the localization and classification of lesions compared with PET imaging alone. Integrated PET/CT has been successfully established in clinical workflow since this multimodality imaging was introduced. The role of PET/CT imaging is increasing in clinical oncology and patient care [1–4].

Likewise, concepts for a PET scanner combined with magnetic resonance (MR) imaging have emerged, replacing CT. The MR data yields high soft tissue contrast and can be used to evaluate the brain, bone marrow, liver and soft tissue tumors. An additional advantage of MR over CT is the absence of ionizing radiation exposure. This new hybrid imaging modality can be expected to have a potential value over PET/CT [5–9]. Recently, the first integrated whole-body PET/MR scanner (Biograph mMR; Siemens Medical Solutions, Erlangen, Germany) was introduced. Because there are fundamental differences between CT and MR imaging, these lead to distinct differences between PET/CT and PET/MR, not only regarding image interpretation but also concerning data acquisition, data processing and image reconstruction. A hybrid PET/MR scanner uses avalanche photodiode–lutetium oxyorthosilicate (LSO) PET detectors, which are integrated between the MR body coil and the gradient coils for simultaneous PET and MR acquisition, keeping mutual interference to a minimum [10]. Additional technical breakthrough for the attenuation correction is an attenuation map with four different tissue types (fat, soft tissue, background and lungs) on the basis of a two-point Dixon MR sequence because MR signal is not related to the radiodensity [11]. Recently some studies suggested that the Dixon MR sequence could be reused for anatomic correlation of PET-positive lesions as well as its use for attenuation correction. This MR sequence could cover the whole body with short acquisition time (19 s for each PET bed position) and it showed a comparable value to low-dose CT for anatomic allocation of PET findings throughout the body in the studies of Eiber et al. [12] and Drzezga et al. [13].

The MR data of hybrid PET/MR should provide anatomic information to distinguish physiologic tracer uptake from pathologic findings and morphologic information to differentiate benignancy from malignancy for unpredicted PET findings, similarly to the CT data of PET/CT. The quality of CT data in PET/CT acquisition protocols is dictated by expertise, experience, conditions at the institution and site preferences. In our institution, the CT of PET/CT was done with standard radiation dose and intravenous contrast. Hence, we evaluated the two-point Dixon sequence of hybrid PET/MR for anatomical correlation and morphological delineation of PET-positive lesions compared with contrast-enhanced PET/CT in oncologic patients.

Materials and Methods

Subjects

Of the pool of patients routinely referred to our institute for ^{18}F-FDG PET/CT for staging and follow-up of malignant disorders, patients with informed consent and ability to undergo another scan after the PET/CT examination were selected from July 2012 to August 2012. Twelve patients (mean age, 55.3±9.04 years, three men, nine women) underwent the ^{18} F-FDG PET/CT with contrast enhancement, immediately followed by hybrid PET/MR. Oncologic diagnoses included breast cancer (n=6), lung cancer (n=1), gastric cancer (n=1), pancreatic cancer (n=1), cholangiocarcinoma (n=1), tongue cancer (n=1) and liposarcoma (n=1) (Table 1). This study was approved by the Institutional Review Board of Yeungnam Medical Center.

Image Acquisition

All patients fasted for at least 6 h before the administration of ^{18}F-FDG and blood glucose concentration was confirmed to be less than 150 mg/dl. Patients received an intravenous injection of 403±45 MBq of ^{18}F-FDG and the acquisition was started 85±13 min after injection using a PET/CT scanner (Discovery VCT; GE Healthcare, Milwaukee, WI, USA) containing Bismuth germinate (BGO) crystals for PET and 64-detector-row CT. First, the CT scan was obtained for attenuation correction of the PET/CT with injection of 100 ml nonionic contrast material (Pamiray 300; Taejoon Pharm, Seoul, Korea) at a flow rate of 2 ml/s. The CT parameters were as follows: 120 kV-200 mA, 3.75 mm slice thickness,

Table 1 Patient characteristics

Patient	Sex	Age	Malignancy	PET-positive findings (n)
1	M	55	Lung cancer	Lymph nodes (2)
2	F	61	Stomach cancer (Signet ring)	Bone (5), thyroid (1)
3	F	52	Breast cancer	Thyroid (1), uterus (1)
4	F	50	Breast cancer	No PET- positive findings
5	M	68	Pancreas cancer	Pancreas (1)
6	F	46	Breast cancer	Breast (1), ovary (1)
7	F	44	Breast cancer	Lymph nodes (16), bone (5), skin (3), pleura (3)
8	F	54	Breast cancer	No PET- positive findings
9	F	57	Breast cancer	Lymph nodes (5), lung nodule (1), lung consolidation (1)
10	M	48	Cholangiocarcinoma	Liver
11	F	53	Liposarcoma	Perirenal fascia
12	F	75	Tongue cancer	Lymph nodes (5), facet joint (1)

2.5 mm reconstruction thickness and 512×512 matrix. And then a three-dimensional (3D) mode PET scan followed with seven to nine bed positions at 3 min per bed position. The PET scanner of the PET/CT had an average spatial resolution of 5.0 mm at 1 cm and 5.6 mm at 10 cm from the transverse field of view (FOV) and a maximum sensitivity of 8.5 kcps/MBq at the center of the FOV. Its axial FOV was 15.7 cm. A total acquisition time was approximately 25–30 min per patient for PET/CT, depending on the scan range.

Subsequent to obtaining PET/CT, PET/MR (Biograph mMR; Siemens Medical Solutions, Erlangen, Germany) was performed (125±19 min after injection of ^{18}F-FDG). This system consists of a 3-T MRI scanner with high gradient performance (maximum amplitude, 45 mT/m; maximum slew rate, 200 T/m/s). The PET/MR system is equipped with Total Imaging Matrix coil technology (Siemens Medical Solutions), covering the entire body with multiple integrated radiofrequency surface coils. The PET scanner of the PET/MR had a spatial resolution of 4.4 mm at 1 cm and of 5.2 mm at 10 cm from the transverse FOV and a sensitivity of 13.2 kcps/MBq at the center of the FOV. The axial FOV was 25.8 cm. First, a localizer MR scan was performed to define the bed positions. And then PET and MR for attenuation correction started at the same bed position simultaneously. The PET scan was obtained for 2 min, taking high PET sensitivity of PET/MR into account and a coronal two-point Dixon 3D volumetric interpolated breath-hold examination (VIBE) T1-weighted MR sequence was acquired for 19 s, which was used for the generation of attenuation maps. The parameters for this MR sequence were as follows: integrated parallel acquisition technique; factor, 2; voxel size, 4.1×2.6×3.1 mm (in-plane resolution × slice thickness); repetition time, 3.6 ms, first echo time, 1.23 ms; second echo time, 2.46 ms; matrix, 79×192; number of excitations, 1; FOV, 500 mm; phase FOV, 65.6 %; 1 slab with 128 slices; slice thickness, 3.1 mm; flip angle, 10; bandwidth, 965 Hz/pixel. The software of the MR automatically used the raw images to produce four different images: T1-weighted in-phase, T1-weighted out-of-phase, water-only, and fat-only. The necessary PET attenuation correction is carried out per section by μ–map made with the Dixon MR sequence consisting of these four different images. After completion of the PET acquisition, the table was moved to the next bed position and patients were covered within three to five bed positions. An additional measurement time must be allowed for the measurement and calculation of the attenuation correction for PET and for the shimming of the magnetic field. A total acquisition time was approximately less than 15 min per patient.

A 3D ordered-subsets expectation maximization (3D OSEM) iterative reconstruction algorithm was applied with 2 iterations and 28 subsets for the PET data of the PET/CT, and with 2 iterations and 21 subsets for the PET data of the PET/MR. For PET/CT, a 128×128 matrix and for PET/MR, a 172×172 matrix was used and both PET data were filtered (6 mm in full width at half maximum).

Image Analysis

Two experienced nuclear medicine physicians interpreted the contrast-enhanced PET/CT and hybrid PET/MR images using the dedicated workstation and software (Syngo.via; Siemens Medical Solutions). The readers analyzed the PET/CT and PET/MR images blinded to the results of the other test and clinical information. The PET/MR images were loaded in the mMR General template and any focal ^{18}F-FDG uptake exceeding normal regional tracer accumulation was assessed as a lesion on the PET images, whether it was malignancy or not. Subsequently, all four coregistered Dixon MR images (T1-weighted in-phase, T1-weighted out-of-phase, fat-only, and water-only) and PET/MR images (fused images of PET data and the water weighted Dixon MR data) were evaluated for anatomic allocation and for the lesion detection corresponding to the focal ^{18}F-FDG uptake. The PET/CT images were loaded in the MM Oncology template and the PET images were reviewed to detect any focal ^{18}F-FDG uptake. The coregistered contrast-enhanced CT images and PET/CT images (fused images of PET data and the contrast-enhanced CT data) were evaluated for anatomic correlation and for the detection of lesions that we primarily identified by ^{18}F-FDG accumulation on the PET image of the PET/CT. If multiple PET-positive lesions were present, lesion counting was limited to a maximum of five hottest lesions per organ system or compartment including lymph node station, according to RECIST criteria and adapted for our purposes. Diagnoses were made in consensus in the event of discrepant diagnoses.

All four Dixon MR images and contrast-enhanced CT image were compared visually by rating the anatomic correlation and morphologic delineation of PET-positive lesions. A scoring scale ranging between 0 and 3 was used for visual ratings (0, no anatomical correlation possible/no morphological correlate detectable; 1, uncertain anatomical correlation/no morphological correlate detectable; 2, good anatomical correlation/questionable morphological correlate; 3, excellent anatomical correlation with a clear morphological correlate) in the same way as a recent publication [12]. In addition, the size of lesion was measured in the best outlining modality.

Mean and maximum SUVs of the all detected lesions were assessed for quantitative comparison on the PET images of both modalities. A volume of interest (VOI) was placed over the PET-positive lesion on the PET images. An iso-contour VOI including all voxels above 40 % of the maximum was created to calculate the SUVmean and the SUVmax was calculated automatically.

Statistics

All statistical analyses were performed using SPSS 19.0 software (SPSS, Chicago, IL, USA). The Kolmogorov–Smirnov test was used to test for a normal distribution. For calculating the overall statistical differences in visual ratings between the contrast enhanced CT and the MR Dixon sequences, we used a nonparametric Friedman test, followed by Wilcoxon signed ranks test with Bonferroni correction for nonnormally distributed samples ($p=0.05$ and $p=0.005$ for Friedman and Wilcoxon signed ranks test, respectively). The Wilcoxon signed ranks test was used to determine the statistical differences in measured SUVs between the two imaging modalities. A p value less than 0.05 was considered statistically significant. The Spearman rank correlation coefficient (ρ) was calculated to examine the correlation between mean and maximum SUVs derived from PET/MR and PET/CT.

Results

Generally, PET results obtained by hybrid PET/MR corresponded with PET results of contrast-enhanced PET/CT (Fig. 1). All patients who had been rated positive or negative for ^{18}F-FDG positive lesions on contrast-enhanced PET/CT were also rated positive or negative on hybrid PET/MR. In 10 of 12 included patients, both hybrid PET/MR and contrast-enhanced PET/CT showed 55 corresponding lesions with focal ^{18}F-FDG accumulation. In total, 28 lymph nodes, 11 bone lesions, 3 dermal nodules, 3 pleural thickening lesions, 2 thyroid nodules, 1 pancreas, 1 liver, 1 ovary, 1 uterus, 1 breast, 1 soft tissue and 2 lung lesions were observed (Table 1).

For the 55 PET-positive lesions, the SUVs (mean and maximum) measured in hybrid PET/MR data (SUVmean, 2.63±1.62; SUVmax, 4.30±2.88) presented a significant decrease (SUVmean, $p<0.001$; SUVmax, $p<0.001$) compared with contrast-enhanced PET/CT data (SUVmean, 3.88±2.30; SUVmax, 6.53±4.04). A mean reduction of 32.44±15.64 % was found in the SUVmean of hybrid PET/MR compared with contrast-enhanced PET/CT, with a range from −2.27 to 87.2 %. The mean value of SUVmax derived from hybrid PET/MR was 35.16±12.59 % lower than that obtained from contrast-enhanced PET/CT, with a range from 9.04 to 77.07 %. However, quantitative evaluation revealed a high correlation between mean and maximum SUVs measured with hybrid PET/MR and contrast-enhanced PET/CT (SUVmean, $\rho=0.93$, $p<0.001$; SUVmax, $\rho=0.95$, $p<0.001$) (Fig. 2).

On the basis of the visual ratings, the contrast enhanced CT scan presented the best performance for anatomic correlation and delineation of PET-positive lesions (mean rating, 2.64±0.70). A significant difference was observed in the scores between contrast-enhanced CT image and all four Dixon MR images, respectively (in-phase, $p<0.001$; opposed-phase, $p<0.001$; water-weighted, $p<0.001$; fat-weighted, $p<0.001$). The water-weighted images (mean rating, 1.71±1.07) were rated the highest among the four Dixon MR images significantly (in-phase, $p=0.001$; opposed-phase, $p<0.001$; fat-weighted, $p<0.001$). The in-phase and opposed-phase images had similar ratings (mean rating: in-phase, 1.29±1.01; opposed-phase, 1.29±1.15), without a significant difference ($p=0.905$). Additionally the fat-weighted images showed the worst score (mean rating, 0.56±1.03). For anatomic correlation of lymph nodes, contrast-enhanced CT scan showed significantly better result than the others (Fig. 3, Table 2). The subjective rating of the bone lesions revealed no significant difference between values obtained for both modalities except a matched pair of contrast-enhanced CT and fat-weighted images (Table 2).

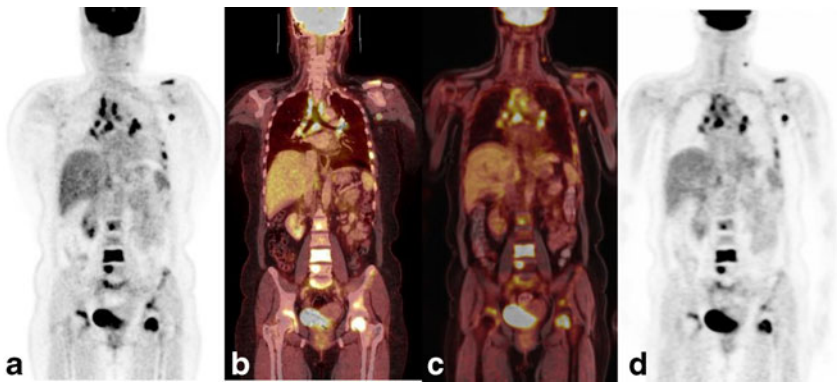

Fig. 1 A 44-year-old woman with multiple metastases from breast cancer underwent a single injection and dual-imaging protocol, contrast-enhanced PET/CT and hybrid PET/MR. **a** ^{18}F-FDG PET image acquired on PET/CT. **b** Fusion of PET data and contrast-enhanced CT data acquired on PET/CT. **c** Fusion of PET data and water-weighted Dixon MR data acquired on hybrid PET/MR. **d** ^{18}F-FDG PET image acquired on hybrid PET/MR. A high reproducibility of ^{18}F-FDG-positive lesions could be seen in the mediastinum, left axilla, left neck and multiple bones between **a** and **d**

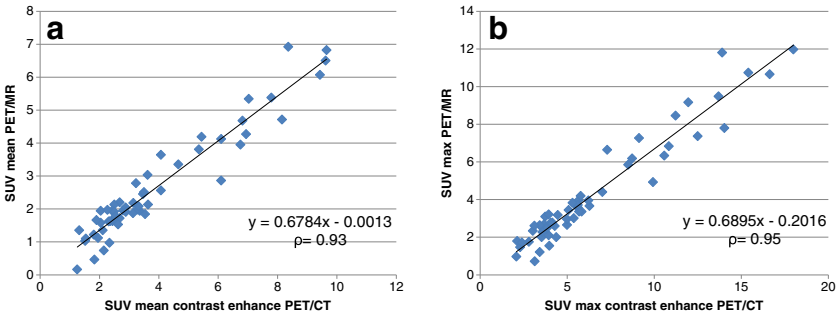

Fig. 2 Correlation analysis of SUVmean (**a**) and SUVmax (**b**) between contrast enhanced PET/CT and subsequent hybrid PET/MR in PET positive lesions. High correlation exists between quantitative values from both modalities (ρ = Spearman rank correlation coefficient)

Discussion

With the recent introduction of hybrid PET/MR, a new multimodality system is undergoing clinical validation compared with PET/CT which was the first realization of a multimodality clinical imaging system. In our study, the PET component of the hybrid PET/MR reproduced ^{18}F-FDG-avid lesions that were detected on the contrast-enhanced PET/CT. Moreover, quantitative evaluation revealed a strong correlation between the SUVs measured in hybrid PET/MR and contrast-enhanced PET/CT (SUVmean, ρ=0.93; SUVmax, ρ=0.95). A higher PET sensitivity of hybrid PET/MR (13.2 kcps/MBq) compared with PET/CT (8.5 kcps/MBq) allowed equivalent performance despite shorter acquisition time (2 min per bed position) and delayed start time of the hybrid PET/MR acquisition.

For details of quantitative analysis, the SUVs measured in hybrid PET/MR presented a significant decrease compared with contrast-enhanced PET/CT confirming recently published results. However, our data showed more prominent reduction of SUV values than other studies with about 10 % [12–14]. This discrepancy may be due to different inclusion criteria of lesions. Whereas previous studies included ^{18}F-FDG-avid lesions suspicious for malignancy, our study included any focal ^{18}F-FDG uptake, whether it was malignancy or not. Because unpredicted PET findings may be detected anywhere, anatomic and morphologic information may also be necessary to define the lesion even though it is benign. However, tracer clearance was more affected in benign lesions than in malignant lesions with time [15–17]. This may cause a greater SUV decrease in our data. Previous studies also demonstrated a large SUV decrease, with a range from 24.5 to 45.13 %, although in the background measurements [13, 14, 18]. Apart from biological explanations, there are also technical factors for the differences in SUV. In contrast with previous studies using scanners from the same manufacturers, we used scanners from different manufacturers, which usually have different hardware, acquisition protocols, image reconstruction algorithms, and data analysis software. SUV measurements are not highly reproducible across different scanner types [19, 20]. However, we interpreted the images using the same data analysis software for the same VOI methodology. Another potential cause of different SUV values is the use of contrast-enhanced CT for PET attenuation correction. Because intravenous contrast agents may lead to overestimation of attenuation, higher SUVs may occur. However, Berthelsen et al. [21] indicated that although the

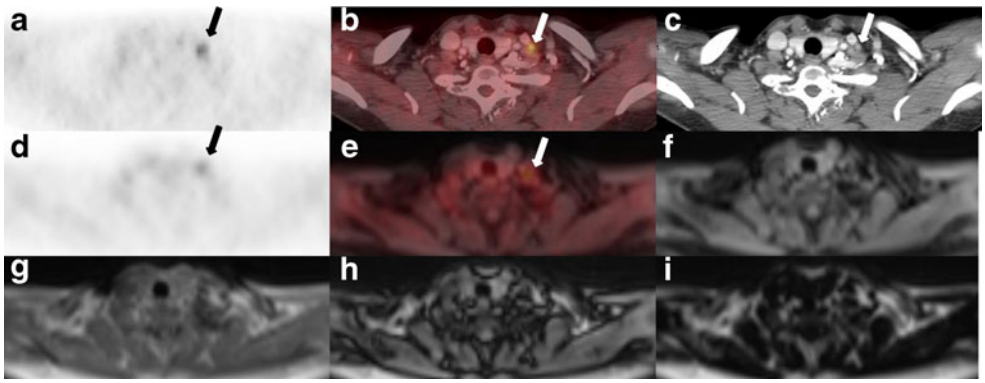

Fig. 3 A 57-year-old woman with breast cancer. Focal uptake of left neck was found both ^{18} F-FDG PET images acquired on contrast-enhanced PET/CT (**a**) and on hybrid PET/MR (**d**). Contrast-enhanced PET/CT image (**b**) presented left cervical lymph node uptake with excellent anatomical correlation and clear morphological delineation could be found on the contrast enhanced CT image (**c**). Hybrid PET/MR image (**e**) and four different coregistered Dixon MR images (**f** water-only, **g** T1-weighted in-phase, **h** T1-weighted out-of-phase and **i** fat-only) presented no morphological correlate of focal ^{18}F-FDG uptake and uncertain anatomical correlation because of blurry delineation with background structures including adjacent blood vessels

Table 2 Anatomical correlation and delineation of PET-positive findings according to anatomic region

Lesion type		*n*	Size (mm)	SUVmean in PET/CT	SUVmean in PET/MR	Contrast-enhanced CT scoring	MR scoring			
							In-phase	Opposed-phase	Water-weighted	Fat-weighted
Lymph node	All	28	10.53±6.25	3.85±2.20	2.65±1.60	2.54±0.74	1.21±0.99[a]	1.21±1.13[a]	1.54±1.04[b]	0.79±1.17[a]
	Neck	6	7.42±2.48	2.85±0.77	1.99±0.65	3	1.17±0.75	1±1.10	1.17±0.75	1.17±0.98
	Thorax	19	12.09±6.94	4.38±2.48	2.97±1.84	2.42±0.84	1.42±1.02	1.47±1.12	1.84±1.01	0.79±1.27
	Abdomen	3	6.83±2.50	2.46±0.21	1.93±0.29	2.33±0.58	0	0	0.33±0.58	0
Bone		11		5.49±2.91	3.55±1.95	2.82±0.40	1.73±1.01	1.91±1.04	2.27±1.10	0.36±0.92[c]

[a] Significantly lower scores compared with contrast-enhanced CT ($p<0.001$)

[b] Significantly lower scores compared with contrast-enhanced CT ($p=0.001$)

[c] Significantly lower scores compared with contrast-enhanced CT ($p=0.003$)

overall increase in the SUVmean was 4.5 %, CT scans with intravenous contrast agent can be used for attenuation correction of the PET data in PET/CT scanning, without changing the clinical diagnostic interpretation. Our study showed high reproducibility of the two modalities, with a strong correlation between the SUVs measured with hybrid PET/MR and contrast-enhanced PET/CT, although there was an SUV discrepancy. Because the given various factors can cause differences in SUV measurement, the status of intravenous contrast agent and scanner type must be taken into account for quantitative use of SUV in treatment evaluation. The use of the same hybrid PET/MR for baseline and follow-up examinations may also be a solution.

For anatomic localization of PET-positive lesions, the two-point Dixon VIBE sequence and the contrast-enhanced CT were evaluated by using the subjective rating. The contrast-enhanced CT scan presented the best performance for anatomic correlation and depiction of PET-positive lesions significantly compared with all four Dixon MR images in our study. Our data showed lower MR scores than other studies [12, 13] and it was probably due to a different proportion of the type and location of lesions. About half of all included lesions were lymph nodes in our study. Moreover, these were small in size. We performed statistical analysis according to anatomic region partially because of the limited number of different lesion types. For anatomic correlation of lymph nodes, the contrast-enhanced CT scan showed significantly better result than the others. When lymph nodes were small and located at anatomically complex areas, the contrast-enhanced CT offered more precise anatomic background information and more improved delineation of lesions from adjacent blood vessels, organs, and muscles by increasing attenuation differences. The subjective rating of the bone lesions revealed no significant difference between values obtained for both modalities, except for a matched pair of contrast-enhanced CT and fat-weighted images. The Dixon MR images provided indistinct outline resulting from low spatial resolution, whereas the contrast-enhanced CT presented clear outline and characterization of the lesion.

Based on our results, the Dixon MR sequences used for attenuation correction are insufficient for anatomic allocation of PET images. Eiber et al. [12] also discussed the limitation of the Dixon MR sequence with lower spatial resolution compared with low-dose CT. To improve the efficiency and to be successfully established in clinical workflow, hybrid PET/MR imaging should not cause diagnostic degradation in either the MR or PET imaging. Concerning the MR protocol, compromises on time might result in a decrease of full individual performance and advantages. Anatomic background information from MR image plays an important role in interpreting PET findings especially in unpredicted PET positive findings because there are no other reference images. Thus, additional MR sequence covering the whole body with acceptable quality may be necessary for anatomic information.

Our study has some limitations. First, PET/CT and PET/MR scans were not obtained at the same time, which could induced the change of ^{18}F-FDG uptake in the benign and malignant lesions. Second, we did not provide a "gold standard" based on histopathology or follow-up imaging for the lesions detected on PET. However, this study included any focal ^{18}F-FDG uptake as a lesion, whether it was malignant or not. In addition, the aim of our study was not to provide a specific diagnosis but to compare the anatomic allocation of hybrid PET/MR and contrast-enhanced PET/CT in delineation of PET-positive lesions. This study could be considered preliminary because the clinical performance of the two modalities was not compared in a well-defined clinical indication, concerning lesion type and primary tumor. However, our data may form the necessary foundation for further studies to find optimized hybrid PET/MR protocols and to validate clinical values of hybrid PET/MR in various indications.

Conclusions

Despite different scanner geometry and attenuation correction approaches, hybrid PET/MR and contrast-enhanced PET/CT are highly reproducible in qualitative lesion detection. The SUV values of PET-positive lesions correlated well between hybrid PET/MR and contrast-enhanced PET/CT, although hybrid PET/MR presented lower SUV values. The Dixon MR images acquired for attenuation correction were insufficient for anatomic allocation of PET images because of low spatial resolution. Thus, additional MR sequence covering the whole body with fast and higher resolution may be necessary for anatomic information.

Conflicts of Interest The authors declare no conflict of interest.

References

1. Collins CD. PET/CT in oncology: for which tumours is it the reference standard? Cancer Imaging. 2007;7:77–87. Spec No A.
2. Czernin J, Allen-Auerbach M, Schelbert HR. Improvements in cancer staging with PET/CT: literature-based evidence as of september 2006. J Nucl Med. 2007;48 Suppl 1:78S–88S.
3. Bar-Shalom R, Yefremov N, Guralnik L, Gaitini D, Frenkel A, Kuten A, et al. Clinical performance of PET/CT in evaluation of cancer: additional value for diagnostic imaging and patient management. J Nucl Med. 2003;44:1200–9.
4. Antoch G, Saoudi N, Kuehl H, Dahmen G, Mueller SP, Beyer T, et al. Accuracy of whole-body dual-modality fluorine-18-2-fluoro-2-deoxy-D-glucose positron emission tomography and computed tomography (FDG-PET/CT) for tumor staging in solid tumors: comparison with CT and PET. J Clin Oncol. 2004;22:4357–68.
5. Buchbender C, Heusner TA, Lauenstein TC, Bockisch A, Antoch G. Oncologic PET/MRI, part 1: tumors of the brain, head and neck, chest, abdomen, and pelvis. J Nucl Med. 2012;53:928–38.
6. Buchbender C, Heusner TA, Lauenstein TC, Bockisch A, Antoch G. Oncologic PET/MRI, part 2: bone tumors, soft-tissue tumors, melanoma, and lymphoma. J Nucl Med. 2012;53:1244–52.
7. Schlemmer HP, Pichler BJ, Krieg R, Heiss WD. An integrated MR/PET system: prospective applications. Abdom Imaging. 2009;34:668–74.
8. Wehrl HF, Judenhofer MS, Wiehr S, Pichler BJ. Pre-clinical PET/MR: technological advances and new perspectives in biomedical research. Eur J Nucl Med Mol Imaging. 2009;36 Suppl 1:S56–68.
9. Antoch G, Bockisch A. Combined PET/MRI: a new dimension in whole-body oncology imaging? Eur J Nucl Med Mol Imaging. 2009;36 Suppl 1:S113–20.
10. Delso G, Furst S, Jakoby B, Ladebeck R, Ganter C, Nekolla SG, et al. Performance measurements of the Siemens mMR integrated whole-body PET/MR scanner. J Nucl Med. 2011;52:1914–22.
11. Martinez-Moller A, Souvatzoglou M, Delso G, Bundschuh RA, Chefd'hotel C, Ziegler SI, et al. Tissue classification as a potential approach for attenuation correction in whole-body PET/MRI: evaluation with PET/CT data. J Nucl Med. 2009;50:520–6.
12. Eiber M, Martinez-Moller A, Souvatzoglou M, Holzapfel K, Pickhard A, Loffelbein D, et al. Value of a dixon-based MR/PET attenuation correction sequence for the localization and evaluation of PET-positive lesions. Eur J Nucl Med Mol Imaging. 2011;38:1691–701.
13. Drzezga A, Souvatzoglou M, Eiber M, Beer AJ, Furst S, Martinez-Moller A, et al. First clinical experience with integrated whole-body PET/MR: comparison to PET/CT in patients with oncologic diagnoses. J Nucl Med. 2012;53:845–55.
14. Wiesmuller M, Quick HH, Navalpakkam B, Lell MM, Uder M, Ritt P, et al. Comparison of lesion detection and quantitation of tracer uptake between PET from a simultaneously acquiring whole-body PET/MR hybrid scanner and PET from PET/CT. Eur J Nucl Med Mol Imaging. 2013;40:12–21.
15. Demura Y, Tsuchida T, Ishizaki T, Mizuno S, Totani Y, Ameshima S, et al. 18F-FDG accumulation with PET for differentiation between benign and malignant lesions in the thorax. J Nucl Med. 2003;44:540–8.
16. Zhuang H, Pourdehnad M, Lambright ES, Yamamoto AJ, Lanuti M, Li P, et al. Dual time point 18F-FDG PET imaging for differentiating malignant from inflammatory processes. J Nucl Med. 2001;42:1412–7.
17. Chan WL, Ramsay SC, Szeto ER, Freund J, Pohlen JM, Tarlinton LC, et al. Dual-time-point (18)F-FDG-PET/CT imaging in the assessment of suspected malignancy. J Med Imaging Radiat Oncol. 2011;55:379–90.
18. Heusch P, Buchbender C, Beiderwellen K, Nensa F, Hartung-Knemeyer V, Lauenstein TC, et al. Standardized uptake values for [(18)F] FDG in normal organ tissues: comparison of whole-body PET/CT and PET/MRI. Eur J Radiol. 2013;82:870–6.
19. Boellaard R. Standards for PET image acquisition and quantitative data analysis. J Nucl Med. 2009;50 Suppl 1:11S–20S.
20. Westerterp M, Pruim J, Oyen W, Hoekstra O, Paans A, Visser E, et al. Quantification of FDG PET studies using standardised uptake values in multi-centre trials: effects of image reconstruction, resolution and ROI definition parameters. Eur J Nucl Med Mol Imaging. 2007;34:392–404.
21. Berthelsen AK, Holm S, Loft A, Klausen TL, Andersen F, Hojgaard L. PET/CT with intravenous contrast can be used for PET attenuation correction in cancer patients. Eur J Nucl Med Mol Imaging. 2005;32:1167–75.